

REGIONAL FORCING OF GREENLAND ICE LOSS

2002–2017

Benjamin Getraer

A JUNIOR PAPER
PRESENTED TO THE FACULTY
OF PRINCETON UNIVERSITY
IN CANDIDACY FOR THE DEGREE
OF BACHELOR OF ARTS

RECOMMENDED FOR ACCEPTANCE
BY THE DEPARTMENT OF
GEOSCIENCES
Adviser: Frederik J. Simons

May 9, 2018

This paper represents my own work in accordance with University regulations,

Benjamin Getraer

Abstract

Melting ice from the Greenland Ice-Sheet accounts for over 20% of rising sea-levels. As recently as 2016, gravimetric and altimetric studies of Greenland melting rates found increasing rates of ice loss, which have not been borne out in observations over the last few years (2015–2017). We hypothesize that the true trend of Greenland ice loss is linear, and that deviations from the linear trend may be explained by inter-annual variability in climate recorded in regional sea surface temperature and atmospheric pressure. We use spatially and spectrally concentrated spherical harmonic solutions for surface mass anomalies to map inter-annual variability across Greenland. We investigate the potential of discrete wavelet analysis to derive spatial structure of inter-annual variability. Unexpected periodic structure of 3–7 years are found in the mass trend of specific regions of Greenland defined by the wavelet basis, and we are able to locate the 2012–2014 anomaly in spatial scale and location, variability that we hypothesize to be strongly correlated with local weather conditions.

Key Points:

1. We focus on inter-annual variability of the Greenland ice loss trend.
2. We analyze subregional signals using discrete wavelet transforms.
3. We find unexpected periodic structure of 3–7 years in the Greenland ice loss trend.
4. We define the 2012–2014 anomaly in spatial structure.

Acknowledgements

Thank you to my adviser Prof. Frederik J. Simons who helped me with the conceptualization, direction, and revision of this project. Thank you to the second reader of my Fall Junior Paper, Prof. Jessica Irving for feedback, suggestions, and encouragement. Thanks to Dr. Amanda Irwin Wilkins and “The Hare” writing workshop group for discussing and editing various figures and drafts. Thank you to Prof. Adam C. Maloof who taught me L^AT_EX, and to Dr. Chris Harig for providing some of the data files. Thank you to Prof. Gabriel Vecchi for insight into atmospheric and oceanic processes. Thank you to Jean Getraer, Andrew Getraer, Jonathan Feld, Rae Perez, and Zach Smart for proof-reading various drafts. Lastly, thank you to the numerous professors and graduate students in the Princeton Department of Geosciences for feedback, encouragement, and constructive criticism on the presentation of preliminary results.

Contents

Abstract	iii
Acknowledgements	iv
List of Figures	vi
List of Tables	vii
Main Text	1
Introduction	1
Methods	4
Expansion of the GRACE signal in space and time	4
Wavelet decomposition of the 2-D spatial signal	7
Results	11
The Greenland time series	12
Conclusions and Future Work	16
Appendix A: Data sources	18
Appendix B: GRACE, spherical harmonics, and Slepian functions	20
References	24

List of Figures

1	Previous Results: Greenland Ice Loss 2002–2014	2
2	Greenland Mass Trend: 2003–2017	3
3	Comparison of GRACE Trend Residuals to North Atlantic Oscillation	4
4	Slepian-based Seasonal Model of Greenland Mass	6
5	The Discrete Grid Around Greenland	8
6	Wavelet Comparisons on the Test Image	9
7	Wavelet Reconstruction with Thresholding and Masking	11
8	Greenland Time Series Reconstruction in the Wavelet Basis: Bias Correction . .	12
9	Example of a Temporally Modeled Wavelet Coefficient	13
10	Greenland Time Series Reconstruction in the Modeled Wavelet Basis	14
11	Significance of Periodic Structure in Model Residuals	15
13	Greenland Time Series in the Altered Modeled Wavelet Basis	17
14	Location of the 2012–2014 Deviation	18
15	Comparison of Spherical Harmonic Eigenfunctions to Slepian Basis Eigentapers	21

List of Tables

1	Expansion Equations for GRACE Data	5
2	The Wavelet Basis Expansion	7
3	Variance and Bias Equations	9
4	Wavelet Thresholding	10

Introduction

The accelerating rise of average global surface temperature — approximately 0.09°C per decade between 1880 and 2012, and approximately 0.26°C per decade between 1979 and 2012 (Hartmann et al., 2013) — has caused a reduction in the mass of the cryosphere, including sea ice and temperate glaciers (approximately -4% per decade and -300 Gt per year, respectively; Vaughan et al., 2013), as well as the Greenland and Antarctic ice sheets (approximately -244 Gt and -92 Gt per year, respectively; Harig & Simons, 2015, 2016). Massive loss of ice has significant repercussions for human civilization, bringing with it a rising sea level at about 1–2 mm per year at the end of 2010 (Church et al., 2013). The Greenland Ice Sheet covers just over 1% of Earth’s surface, and, if completely melted, would raise sea level by over 7 m (Vaughan et al., 2013). We seek to understand deviations from modeled rates of Greenland ice melt in order to better understand, predict, and communicate the changing conditions of the planet.

Previous studies have modeled ice mass on the Greenland Ice Sheet using gravimetric data from NASA’s Gravity Recovery and Climate Experiment (GRACE), as well as satellite and airplane based altimetry, finding decreasing rates in the ice mass signal over the last decade (Harig & Simons, 2016; Khan et al., 2015). Rates of ice loss increase by a combination of greater discharge, from calving glacier termini at the edges of the ice-sheet, and decreased surface mass-balance, the difference between seasonal snow accumulation and melting (Enderlin et al., 2014; Khan et al., 2015). Significant inter-annual variability and asynchronicity has been observed in the discharge rates of the Greenland Ice Sheet’s major drainage basins, while surface mass-balance is comparatively more predictable (Enderlin et al., 2014; McMillan et al., 2016). Both contributions to ice loss accelerated between 2000–2012, combining for a total acceleration of ice mass estimated around -30 Gt per year² over all of Greenland (Enderlin et al., 2014; Velicogna, 2009).

A recent study by Harig & Simons (2016) modeling the mass of the Greenland Ice Sheet using GRACE data products showed deviations from the long-term quadratic trend, starting with a high level of melt in the summer of 2012, and followed by two summers of little melting in 2013

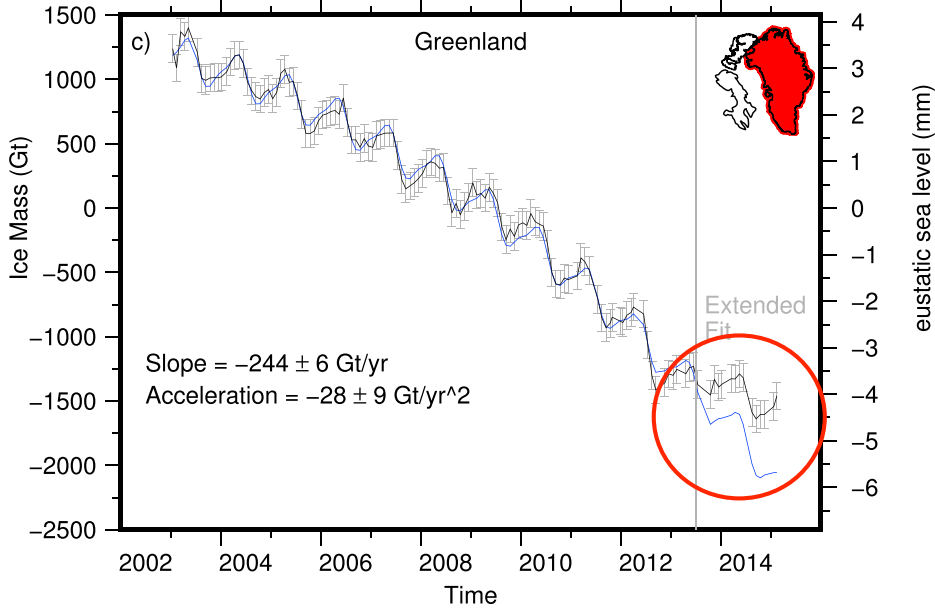


Figure 1: Total ice mass changes calculated using GRACE RL05 data products (see Appendix A: Data sources) and a Slepian basis for Greenland (see Appendix B: GRACE, spherical harmonics, and Slepian functions) with a coastal buffer of 0.5° (inset), adapted from Harig & Simons (2016), their Figure 4. Shown is the variation of the GRACE observations (black) from the modeled trend (blue) — note the significant departure of the 2014 GRACE observations from the extrapolated trend of the apparent acceleration of the previous decade (circled in red).

and 2014 (see Figure 1, adapted from Harig & Simons, 2016, their Figure 4). These deviations have been connected to atmospheric forcing from the North Atlantic Oscillation (NAO), suggesting that the changes from the expected mass balance were driven by summer surface mass balance as opposed to terminus discharge rate (see Bevis et al., 2018; McMillan et al., 2016).

Building upon the results and unresolved questions from Harig & Simons (2016), we applied their method of spherical Slepian basis modeling to the years that have passed since. Significantly, our analysis of the complete GRACE data set (2002–2017) showed a linear, not accelerating, trend of ice loss for the Greenland Ice Sheet (see Figure 2). Comparison of the residuals of the linear model of ice-sheet melt to the NAO generally confirms correlations found by McMillan et al. (2016) and Bevis et al. (2018) and suggests that the residuals of the linear model are indeed related to inter-annual atmospheric forcing of the NAO and not part of the long-term trend (see Figure 3).

In this project, we investigate the inter-annual variability of the Greenland Ice Sheet, defined as structured signal that cannot be modeled as having constant, linear, quadratic, cubic, annually, or semiannually periodic temporal structure, in a geographic context. To achieve spatial localization, we develop a discrete wavelet basis for decomposing GRACE spherical harmonic solutions evaluated on a grid around Greenland, and we model each wavelet coefficient through time. We find that there exists significant unexplained periodic structure contained within some of the wavelet coefficients, with regions located in the northwest and southeast of Greenland manifesting periods of approximately 3–7 years.

We find that the signal of the 2012–2014 anomalies is spatially localized to Northern and Northwestern Greenland.

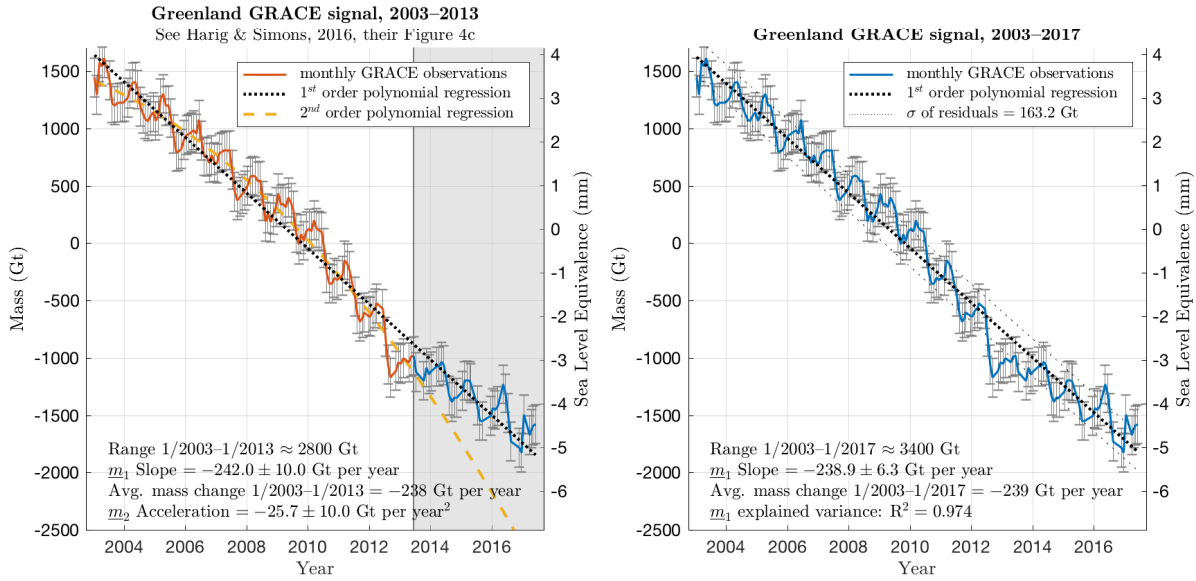


Figure 2: Total mass changes for Greenland over the complete GRACE record using equivalent methods to Harig & Simons (2016). Shown in **A** are the m_1 linear and m_2 quadratic models for 01/2003–06/2013, comparable to previous estimates of the mass trend (see Figure 1). Note the significant departure of the extrapolated m_2 model from the continuing signal. Shown in **B** is the m_1 linear model for 01/2003–06/2017 with the standard of deviation of its residuals. Note that the m_1 model does not significantly change after including the entire GRACE record. Error bars represent 2σ based on the combined variance of modeled Slepian coefficients f_{α} (see 9 for equivalent usage in our wavelet model). This Figure appeared in my Fall JP, here with minor updates.

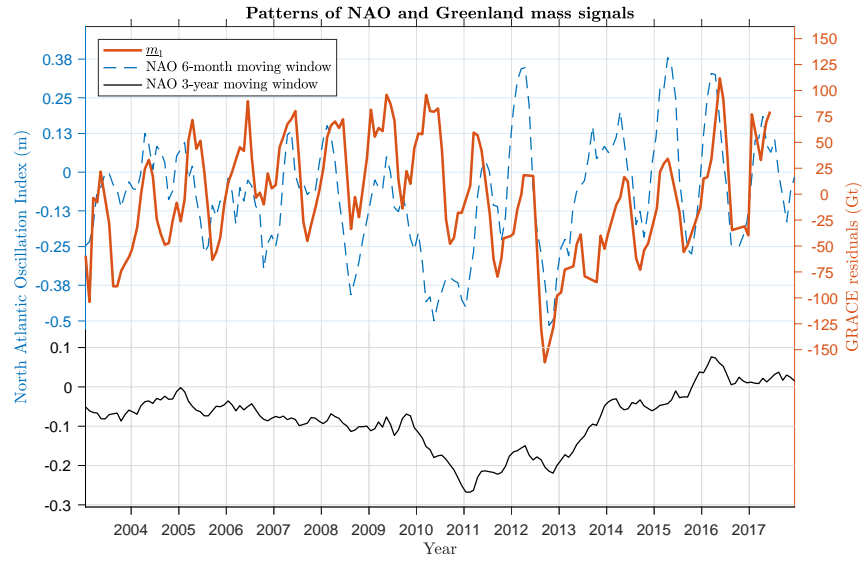


Figure 3: Residuals from our m_1 model of the Greenland mass signal compared to 6-month and 3-year moving averages of the NAO index (see Appendix A: Data sources). On top, note the seasonal rising and falling of the Greenland Ice Sheet mass in the model residual, and that the mass is correlated with the 6-month NAO signal, especially from 2012 onwards. The steep drop in ice mass in 2012 that marked the beginning of the 2012–2014 anomaly coincided with a steep drop between two extremes of the NAO index, while the little melt in 2013 coincided with a sustained high NAO index that summer. On bottom, notice the decline of the 3-year NAO index from 2005–2011, and its general rise from 2013–2017. These long-term signals are coincident with the general long-term structure of the residuals as well. This Figure appeared in my Fall JP.

Methods

Our study uses a time series of surface mass density of the Greenland Ice Sheet from data collected by the GRACE satellite mission and made publicly available as global spherical harmonic coefficients by NASA in the CSR-RL05 data product (see Appendix A: Data sources). For a description of spherical harmonics and Slepian functions with regards to GRACE measurements, see Appendix B: GRACE, spherical harmonics, and Slepian functions.

Expansion of the GRACE signal in space and time

The gravitational field captured by the GRACE data is a signal with spatial and temporal structure. Note that determining how the spatial structure of the signal evolves over time is fundamentally different from determining how the temporal structure of the signal evolves in space. There exists a significant tradeoff between variance and bias in attempting to know both the

Approximation method	Expansion Equations	Spatial Support
Spherical Harmonic	$M_{SH}(\underline{r}) = \sum_{l=0}^L \sum_{m=-l}^{+l} f_{lm} Y_{lm}(\underline{r})$	global
Slepian Functions	$M_{SF}(\underline{r}) = \sum_{\alpha=1}^N f_\alpha g_\alpha(\underline{r})$	concentrated
Wavelet Basis	$M_{WB}(\underline{r}) = \sum_{\beta=1}^K m_\beta w_\beta(\underline{r})$	compact

Table 1: Expansions used to represent the mass density field $M(\underline{r})$. Note that each expansion is a superposition of a basis function (some $F_i(\underline{r})$) weighted by a constant (some c_i). The GRACE CSR RL05 spherical harmonic data have a bandwidth $L = 60$, with a total of $(L + 1)^2 = 3721$ coefficients required to describe the field in any point in space (see Appendix B: GRACE, spherical harmonics, and Slepian functions & Equation 3). In the Slepian expansion over Greenland, the Shannon number is $N \approx 20$, a massive reduction in the coefficients needed to describe the field (see Appendix B: GRACE, spherical harmonics, and Slepian functions & Equation 4). Finally, the wavelet basis is expanded on a square grid of length \sqrt{K} , where K is the total number of wavelets in the complete expansion. By choosing wavelets by thresholded coefficient values and support within Greenland, we develop a partial wavelet reconstruction on a 256×256 grid over Greenland with only 68 coefficients.

spatial attributes (how the mass density of the region is distributed spatially at a single point in time) and temporal attributes (how the total mass of a specific geographic region changes over time) of the GRACE signal. To aid in being “right” on average about the spatial structure, we may average over time, while if we want to be “right” on average about the temporal structure, we can average over space.

In general, we want to extract a combination of temporal and spatial structure from the data, and so we trade resolution (in spatial footprint and temporal duration) for variance (also in space and time). In estimating the total changing mass of Greenland from GRACE, a spatial footprint is often chosen around the entirety of Greenland, accomplished using a weighted spatial masking function (as in Velicogna & Wahr, 2005) or in terms of Slepian eigentapers (as in Harig & Simons, 2016, and Figure 2). In both of these two methods of localized expansion, the GRACE spherical harmonic functions are effectively translated from a basis with global support to a basis with regionally concentrated support that can then be integrated over Greenland to recover the temporal structure at the desired spatial resolution.

However, what if we wish to understand the spatial structure of changing mass that exists *within* the Greenland footprint? Higher spatial resolution has been extracted by modeling the weighting constants on each of the harmonics (see Wouters et al., 2008) or Slepian functions (as in Harig & Simons, 2016, and Figure 2) by fitting low-order polynomial and seasonally

oscillating functions to the weighting coefficient time-series. The model implemented by Harig & Simons (2016) in Figure 1 and implemented here in Figure 4 uses the following model for weighting coefficient \bar{c}_i in the basic expansion structure of $S_i(\underline{r}) = \bar{c}_i F_i(\underline{r})$:

$$\bar{c}_i = a_i + b_i t + c_i t^2 + d_i t^3 + e_i \sin(\omega_{ann} t + \phi_{ann}) + f_i \sin(\omega_{semi} t + \phi_{semi}) \quad (1)$$

As the harmonic and Slepian functions are continuous and nonvanishing over the entirety of Greenland, a model of their coefficients can tell us how the spatial structure evolves in time on average. Yet any such model of either harmonic or Slepian functions fails to indicate precisely where variation from expected temporal structure occurs in space, as that variation is not specifically represented by any one of the spatial functions, but rather by the superposition of many contributing functions.

f_α Model and Residuals

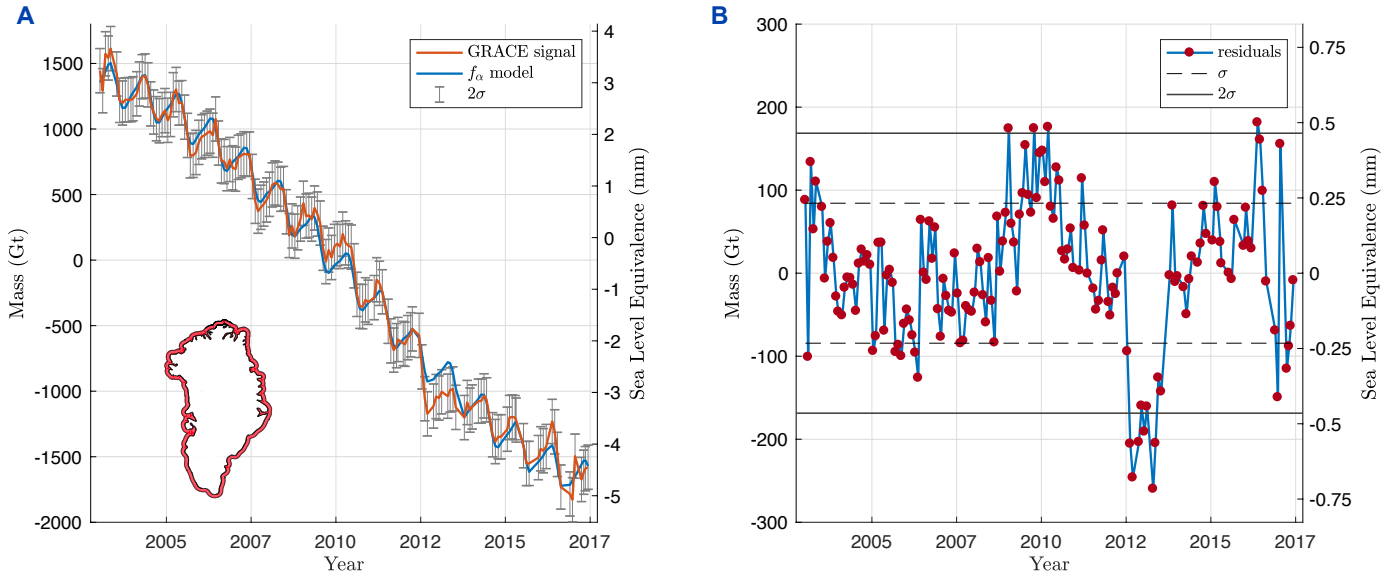


Figure 4: A comparison of the 2003–2017 Greenland mass signal from GRACE with the f_α model of linear and seasonal trends in the Slepian coefficients (see Table 1 & Equation 1). **A** shows the time-series for both the signal and the model, and **B** shows the residuals not explained by Equation 1. 2σ refers to two standards of deviation based on the propagated variance of the residuals of each modeled Slepian coefficient, and represents the best estimate of uncertainty in the Slepian GRACE solution (see Harig & Simons, 2012, their Supporting Information). Note the increase in deviations from the model as compared to the equivalent model by Harig & Simons (2016) seen in Figure 1, and the significant deviations in the de-trended time series in 2009–2010 and 2012–2013. Mass is integrated over Greenland with a coastal buffer of 0.5° (inset). This Figure appeared in my Fall JP.

Over the GRACE time-series we have observed mass fluctuations in Greenland Ice Sheet, specifically between 2012–2014, that we have been unable to localize within Greenland with the typical expansion approaches described above (see Figures 1, 2, & 4). Here we wish to examine this variability that exists within the spatial distribution of the Greenland GRACE signal in order to understand where (in space) and why (in relation to local weather) deviations from the expected trend occur. Recognizing anomalous seasonal behavior such as 2012-2014 is critical to correctly interpreting the long-term trajectory of Greenland ice mass.

Wavelet decomposition of the 2-D spatial signal

In this paper we experiment with a solution to the problem of resolving the spatial variability of Greenland ice loss. We use wavelet analysis of the Greenland mass signal evaluated on a grid, and model the wavelet coefficients through time rather than the spherical harmonic or Slepian coefficients. The expected advantage of this method is that anomalous signals may be traced back to deviations from the trend of specific wavelet coefficients, which by nature inform us of the scale and location of that deviation in space (see Panet et al., 2006). The localizing properties of 2-D wavelets have been used to compare and combine different sources of gravimetry data (see Panet et al., 2006), to differentiate between gravity signals on different spatial scales (see Cadio et al., 2011), and to model local changes in mass anomaly after earthquakes (see Panet et al., 2018). Wavelet bases have also been recommended as a better basis than global spherical harmonics for GRACE Level 1 data reduction (as opposed to model analysis) (Harig et al., 2012).

The wavelet basis expansion

$$M_{WB}(\underline{r}) = \sum_{\beta=1}^K m_{\beta} w_{\beta}(\underline{r}) \quad (1)$$

$$M_{WB}(\underline{r}) = \sum_{\zeta=1}^Z \sum_{\gamma=1}^{\Gamma(\zeta)} m_{\zeta\gamma} w_{\zeta\gamma}(\underline{r}) \quad (2)$$

Table 2: Two equivalent expressions for the superposition of discrete wavelets in two dimensions. We consider Haar wavelets on a $2^n \times 2^n$ cartesian grid. (1) K are the total number of wavelets $K = 2^n$ when expanded to the maximum scale level and β is the wavelet number indexing all wavelets. (2) Z are the number of wavelet decomposition levels, where $Z = n$. ζ is the wavelet level index, where the area of wavelet support at each level is $\int_{\text{support}} w_{\zeta\gamma}(\underline{r}) d\Omega = \zeta^2$ grid cells.

We use discrete wavelet decompositions in two dimensions. Wavelets are oscillating functions with finite support in space. Wavelets of different scales capture signal at different resolution levels, and a discrete implementation of the transform would subsample a spatial grid depending on the scale. Each wavelet at each grid scale is assigned a weighting coefficient such that signal information at a location on the grid can be represented as a superposition of individual wavelets at different scale levels at that point. The weighting m_β associated with the wavelet w_β at each grid point, and at different scales of resolution, tells us where and how important information is at different scales (see Tables 1 & 2).

We begin our wavelet decomposition by defining a $2^8 \times 2^8$ square grid at the center of a face of the “cubed sphere” with 2^{10} surface elements, centered around Greenland (see figure 5). The resulting grid has a spatial resolution of approximately 10 km, far finer than the highest spatial frequency of $L = 60$ spherical harmonics which have a spatial resolution of approximately 170 km, meaning that there is no loss in the spatial signal when evaluated upon the grid.

Next, we choose to use a single image, the difference between the mass density field at either end of the GRACE time-series (January 2003 – June 2017), to develop our wavelet basis (see Figure 7). We make the assumption that the most relevant spatial structures throughout the time-series will be apparent in the total difference from beginning to end.

The discrete wavelet decomposition (analysis) and recombination (synthesis) is a lossless transformation, however many of the wavelet coefficients will have extremely small contributions to the overall image. By thresholding the coefficient values, the data required to reconstruct the original image are greatly reduced. Another advantage to using the total difference

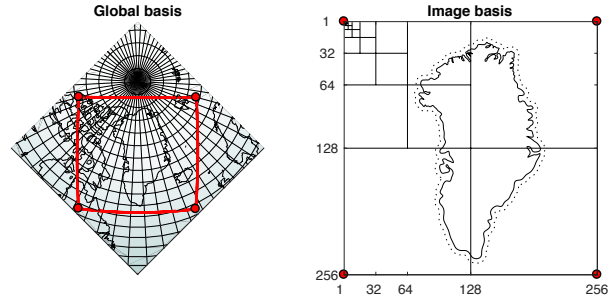


Figure 5: The grid extent around Greenland is defined in the global basis on a face of the cubed sphere centered on Greenland. In the image basis the grid is cartesian with length 256. Grid lines in the image basis represent the diminishing areal support of wavelets of different levels, from $\zeta = 8$ (the entire image) to $\zeta = 1$ (a unit grid cell). Note that in reality, each wavelet level has coverage over the entire image. The dotted line around Greenland is a coastal buffer of 0.5° as in Figures 1, 2, & 4.

over GRACE as our test image is that we have some insight into the overall bias and variance introduced as we threshold the wavelet coefficients. We measure the cost in variance (pixel to pixel error) and bias (summed image pixel value error) which depends on the degree of thresholding (see Table 3).

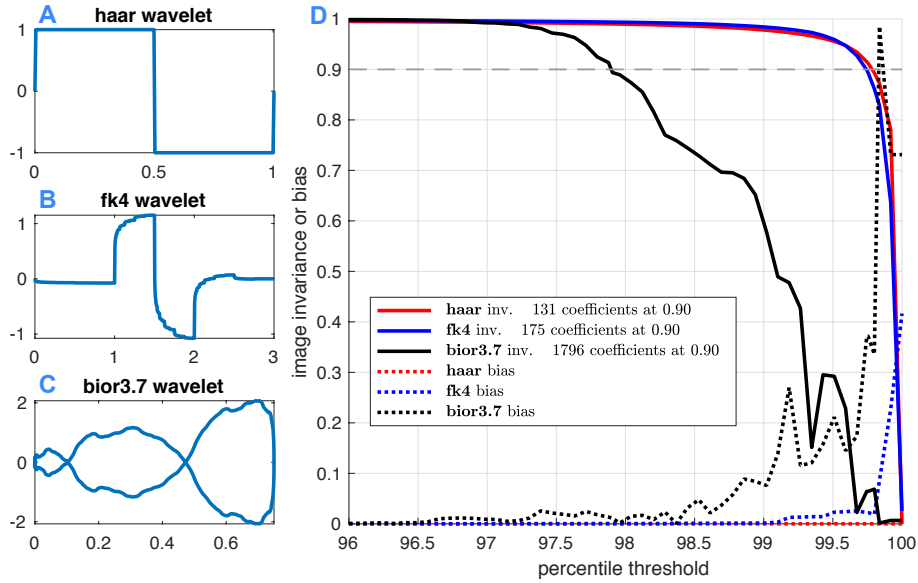


Figure 6: A–C: Cross sections of the Haar (orthogonal), Fejér-Korovkin 4 (orthogonal), and biorthogonal 3.4 wavelets, examples of step-wise, piece-wise, and continuous wavelets of varying orthogonality. D: Performance comparison on the test image, comparing invariance and bias (see Table 3) between the wavelets along coefficient thresholds of different percentiles (see Table 4). Note that at 90% invariance, the Haar wavelet requires significantly fewer coefficients than the others, and that the Haar wavelet also has the best performance in bias — tests that held true for all wavelets tested, leading us to choose the Haar wavelet for our image decomposition.

Next we choose a wavelet to use in the decomposition. Many options are available, however our goal was to retain a large amount of signal structure with a small number of coefficients, which we accomplished using the Haar wavelet (see Table 3 & Figure 6). Using the Haar wavelet, we perform the 2-D deconstruction on our reference image, which breaks down our

Image invariance and bias Equations

$$\text{invar}(A) = 1 - \frac{\text{var}(A_{\text{ref}} - A)}{\text{var}(A_{\text{ref}})} \quad (1)$$

$$\text{bias}(A) = |\text{sum}(A_{\text{ref}}) - \text{sum}(A)| \quad (2)$$

Table 3: (1) Image invariance is a pixel by pixel similarity comparison of an image A against a reference image A_{ref} , where $\text{invar}(A) = 1$ designates an identical picture, and $\text{invar}(A) = 0$ designates an empty picture. (2) Image bias is a comparison of the total summed value of an image A against a reference image A_{ref} , where $\text{bias}(A) = 0$ designates an identical picture, and $\text{bias}(A) > 0$ designates the total pixel value lost. bias is also presented as a percentage of the reference image, i.e. $\text{bias}(A) = |\text{sum}(A_{\text{ref}}) - \text{sum}(A)| \div |\text{sum}(A_{\text{ref}})|$. In regards to our wavelet thresholding in Figures 6 & 7, invar is a measure of how well spatial structure is preserved, while bias is a measure of how well the total Greenland mass signal is preserved. Note that thresholding the wavelet coefficients will cause a decrease in invariance and an increase in bias (see Figure 6).

Wavelet thresholding

(1) Coefficient threshold	$M_{WB}^{\varepsilon}(\underline{r}) = \sum_{\beta=1}^K T_{\varepsilon}(m_{\beta}) m_{\beta} w_{\beta}(\underline{r})$	$T_{\varepsilon}(m_{\beta}) = 1 + H(m = \varepsilon) - H(m = -\varepsilon)$
(2) Basis support threshold	$M_{WB}^{\xi}(\underline{r}) = \sum_{\zeta=1}^Z \sum_{\gamma=1}^{\Gamma(\zeta)} \phi_{\xi(\zeta)}(\rho) m_{\zeta\gamma} w_{\zeta\gamma}(\underline{r})$	$\phi_{\xi(\zeta)}(\rho) = H(\rho = \xi(\zeta))$

where

$$\rho(\zeta) = \frac{\int_G w_{\zeta\gamma}(\underline{r}) d\omega}{\int_{support} w_{\zeta\gamma}(\underline{r}) d\omega}$$

Table 4: Wavelet thresholding Equations based on (1) coefficient value and (2) percentage of wavelet footprint within a 0.5° buffered Greenland (see Figure 5). (1) Threshold function T sets a hard threshold on wavelet coefficients at $|m_{\beta}| = \varepsilon$, shown in **A**. (2) Threshold function ϕ sets a hard threshold on wavelet coefficients at $\rho(\zeta) = \xi(\zeta)$, shown in **B**. ρ is the percentage of wavelet support within Greenland at a given wavelet level, and ξ is the threshold for ρ at that wavelet level. Specifically, we keep all wavelets of the highest two levels ($\xi(\zeta) = 0$) and only those which are 90% inside of Greenland at the highest level ($\xi(\zeta) = 0.9$), with $\xi(\zeta)$ linearly spaced for the levels in between. We use a variable ξ to account for wavelets that have significant coverage within Greenland, despite having most of their support elsewhere. The results of these thresholds can be seen in Figure 7.

image into Haar wavelets of vertical, diagonal, and horizontal orientation at all of our wavelet scale levels. The resultant wavelet coefficients are then thresholded by value and by areal support within Greenland as described in Table 4, choosing threshold values that maintain an invariance of approximately 90% (see Figure 7). We are left with an image reduced to 68 wavelet coefficients and approximately 90% invariance (see Figure 7).

It is important to keep in mind that the “smoothness” of the image created when the spherical harmonic functions are evaluated on a fine grid represents the continuous structure of the functions themselves, and not necessarily the structure of the signal. As shown in Figure 7, much of the smoothness of the signal can be completely removed while retaining a vast majority of the information about spatial structure. The apparent reduction in resolution should not be considered a loss of information, but rather a distillation of the continuous spherical harmonic functions into the important underlying structure that those functions capture.

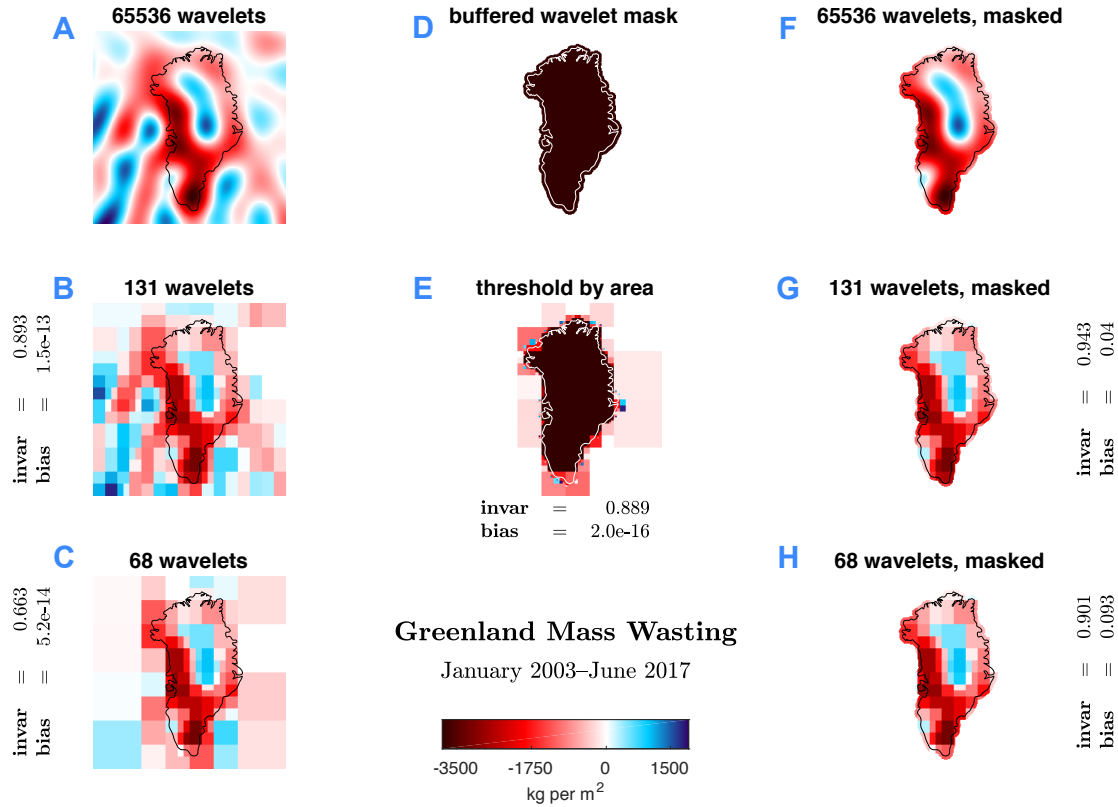


Figure 7: Wavelet reconstruction on the reference image using thresholding defined in Table 4. **A** shows the fully reconstructed image, identical to the spherical harmonics evaluated on the grid, requiring 256×256 wavelets. **B** shows reconstruction of the reference image after thresholding by coefficient value (see Table 4 & Figure 6). **C** shows reconstruction of the reference image after thresholding by coefficient value and areal support within Greenland (see Table 4 & Figure 6). **D** shows the mask of 0.5° buffered Greenland used in calculating the support threshold ϕ and in masking the images. **E** shows a reconstruction of **D** after application of the support threshold ϕ (see Table 4). **F–H** show images **A–C** after masking using image **D**, isolating the Greenland basis for image recovery analysis. Reported invariance and bias are calculated as percentages using Table 3. Thresholds T and ϕ were chosen to achieve approximately 90% image invariance before masking (see Table 4). Note that the final masked and thresholded image **H** is reduced in information to only 68 wavelets, with an invariance of approximately 90% and bias of less than 10% (see Figure 8 for bias correction).

Results

Our results are split into a few different subsections. First, a presentation of the entire Greenland mass time-series integrated in the wavelet basis and modeled through time. Then an analysis of model residuals showing unusual periodic temporal structure. Lastly, a localization of anomalous signal in space.

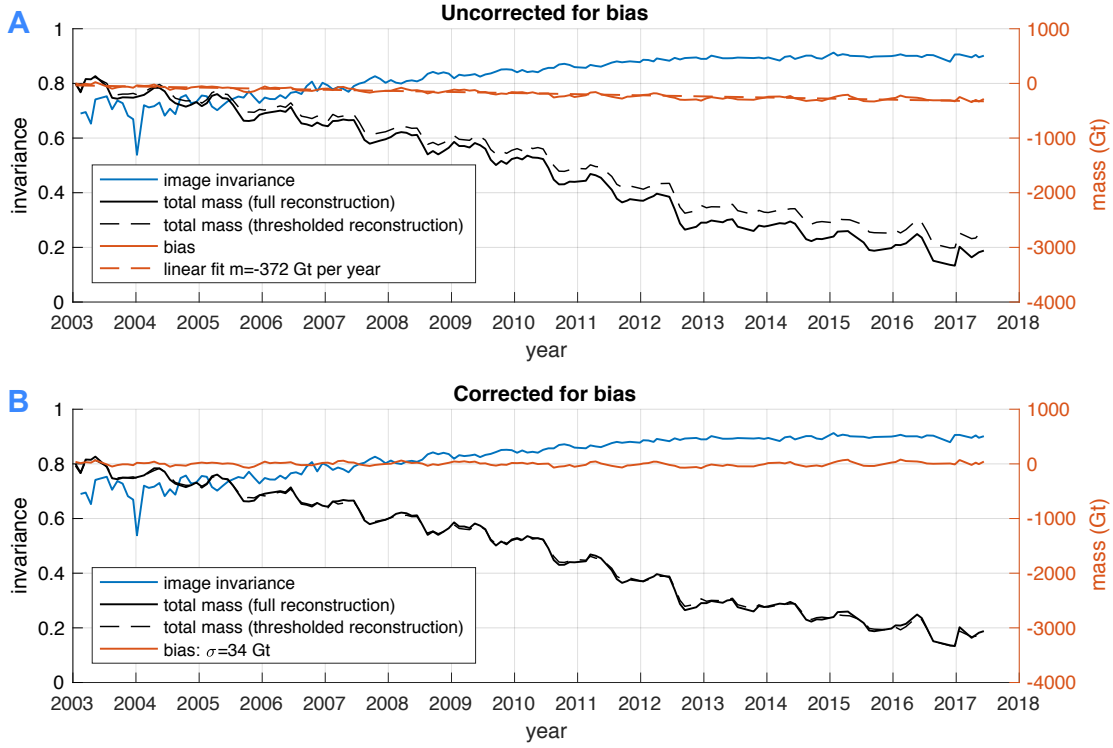


Figure 8: The mass time series of the entire Greenland Ice Sheet in the full wavelet reconstruction (identical to the GRACE spherical harmonic solution) and in the thresholded wavelet reconstruction (see Figure 7). A shows the direct result of thresholding, masking, and summation, including a linear trend in image bias of -373 Gt per year (red), introduced by our thresholding and accumulating because our images are in reference to the beginning of our time series (see Table 3). The invariance measures recovery of spatial structure (blue), which is fairly good (50–70%) in month to month reconstruction (at the beginning of the reconstruction), and very good (approaching 90%) in the beginning to end reconstruction (see Table 3). In B, the linear model of bias shown in A is added back into the total thresholded reconstruction as a correction, with the resultant error having a zero-mean with a standard of deviation of about 1% of the total mass range of the signal.

The Greenland time series

The 68 wavelets chosen through thresholding by weighting magnitude and support location on the reference image (see Wavelet decomposition of the 2-D spatial signal & Figure 7) are used to decompose mass density images on the grid at every time step in the GRACE time-series between January 2003 and June 2017. The wavelet coefficients of the first image in the time-series are then subtracted from every image, such that each image represents cumulative change from January 2003 within our thresholded wavelet basis. After masking each image as shown in Figure 7, each entire image is summed by pixel value to give the total difference in mass at that time-step compared to January 2003 (see Figure 8). Because the difference between each image

is cumulative, the bias of our wavelet reconstruction increases approximately linearly with time at a rate of -373 Gt per year, for which we correct by adding the linearly modeled bias value back in at each time step (see Figure 8 and Equation 2).

Next we model each of the 68 wavelet coefficients of through time based on Equation 1 to capture all constant, linear, quadratic, cubic, annually, or semiannually periodic temporal structure, within the wavelet spatial representation of Greenland (see Figure 9). The mass of Greenland is now represented by the following Equation (see Tables 1 & 2):

$$M_{WB}(\underline{r}, t) = bias(t) + \sum_{\beta=1}^K T_\epsilon \cdot \phi_\xi \cdot (\hat{m}_\beta(t) + n_\beta(t)) \cdot w_\beta(\underline{r}) \quad (2)$$

Where $bias(t)$ is a linear corrective term from Figure 8B, $\hat{m}_\beta(t)$ are our modeled wavelet coefficients following Equation 1, and n are the residuals of the modeled coefficients unexplained by Equation 1 (see Figure 9). We use the modeled coefficients to construct a time series of Greenland mass as we expect it to change with time, which can be seen in Figure 10 (see Figures 1 & 4 for a parallel example in the Spherical harmonic basis).

We can now inspect the spatial locations inter-annual variability of the Greenland Ice Sheet, as any variation from the expected total trend of Greenland (see Figure 10) exists within the residuals n of our wavelet coefficient models at specific scales and locations (see Equation 2).

We expect the residuals n of our coefficient model to be temporally unstructured noise, error, or variability in weather events (see Equation 1). However some of the wavelet coefficient residuals show oscillations in time (see Figure 11D for example).

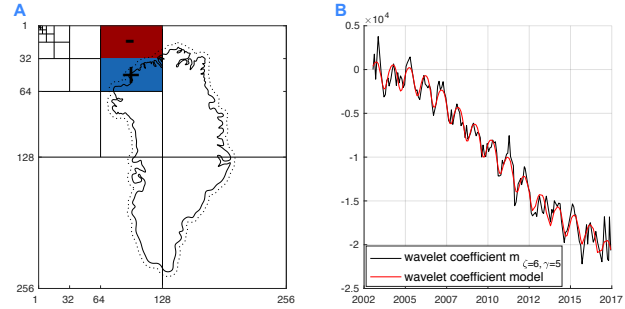


Figure 9: Example of a temporally modeled wavelet coefficient $m_{65}(\underline{r}, t)$ (see Table 2). **A** shows the wavelet spatial support in the image basis, while **B** shows the wavelet coefficient evolution through time with respect to Greenland surface mass density. The coefficient model from Equation 1 is fitted in red, showing a seasonally oscillating decline in the wavelet weighting, which corresponds to a decrease in mass over the positive support of the wavelet in northwestern Greenland (blue in **A**). The coefficient models of each wavelet are summed to produce the modeled time series shown in Figure 10, while the difference between the coefficient model and the decomposition values shown in **B** are summed to produce the residuals in Figure 10. The standards of deviation of the residuals of each of wavelet model are summed as an estimate of noise or error within the reconstruction, shown in the error-bars in Figure 10.

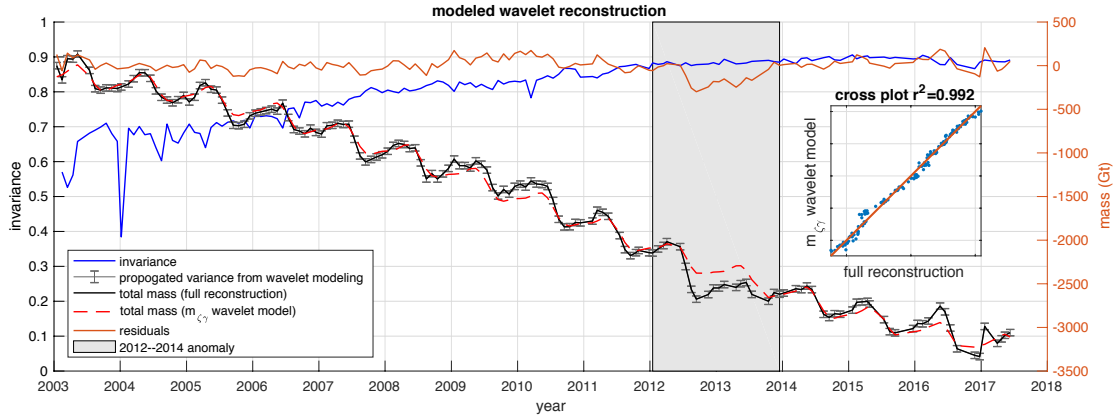


Figure 10: The mass time series of the entire Greenland Ice Sheet in the full wavelet reconstruction (identical to the GRACE spherical harmonic solution, in black) and in the modeled wavelet reconstruction (see Figure 9 and Equation 2, in dashed red). The invariance measures recovery of spatial structure (blue), which is fair (40–70%) in month to month reconstruction (at the beginning of the reconstruction), and very good (approaching 90%) in the beginning to end reconstruction (see Table 3). The residuals are the difference between the full and modeled reconstructions, equal to the $\sum n$ in Equation 2. The error-bars represent 2 standards of deviation with respect to propagated variance from the coefficient model residuals (see Figure 9) and are an estimate of noise and error inherent to the reconstruction (see Figures 1 & 4 for a parallel example in the Spherical harmonic basis). Inset is a cross-plot showing the correlation of the full and modeled reconstructions. Highlighted in gray are the seasons of 2012–2014 which represent the most significant deviation from the expected behavior of the Greenland Ice Sheet within the GRACE record.

We test the significance of these oscillations against the null hypothesis of the residuals $n(t)$ being a set drawn at random from a normally distributed population by bootstrapping. 10,000 sets were drawn at random from a normally distributed population, each set was transformed into a spectral periodogram, and the highest peaks in each set were recorded. Based on these random sets we then define the probability of drawing a set with a given maximum peak value, and use a probability cutoff of $p < 5\%$ to define a set likely to have non-random periodic structure (see Figure 11A).

Out of our 68 wavelet coefficients, 21 were found to have non-random periodic structure ($p < 5\%$), with periods ranging from 3–7 years (see Figure 12). The locations of these periodic residual signals, as well as their phases, are shown in Figure 12. Initial analysis shows that there exists some spatial clustering in the northwestern and southwestern quadrants of Greenland, as well as coherence in phase across wavelet coefficients in the 7 and 5.25 year periods.

Lastly, we examine the widely observed 2012–2014 deviations from the expected trend (see Figures 1, 2, 10, 13, etc). One by one we replace each of the modeled wavelet coefficients in our model for expected temporal behavior (see Figure 13) with the actual coefficients, and inspect

the improvement in our model over the 2012–2014 time period. We find that 4 wavelets account for a large proportion of the variance during those seasons, and can be incorporated into the model by substituting their respective modeled values for real values (see Figure 14). The 2012–2014 deviation is found to exist across all of Greenland, but be concentrated in the southwestern quadrant (see Figure 14).

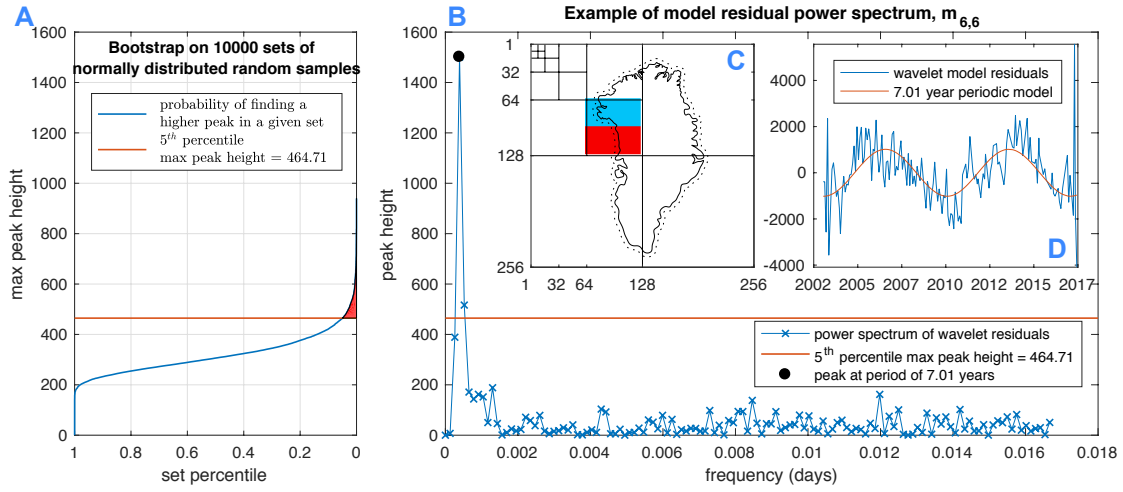


Figure 11: The $n(t)$ residuals of the modeled wavelet coefficients (see example in panel D and Figure 9) were tested for significant periodic structure in time. Panel A illustrates the results of bootstrapping, to test the hypothesis that the $n(t)$ residuals (as in D) are drawn from a random distribution. Periodograms such as in panel B were created to represent the power-spectrum of each randomly drawn set, and the probability of drawing a set with a given maximum peak value was estimated (see panel A). We defined a residual set as having non-random periodic structure if its periodogram contained a peak higher than the 5th percentile of maximum peak heights in our bootstrapping (i.e. < 5% probability of the set being randomly sampled from a normal distribution). B shows the periodogram for the real residual data of wavelet $m_{6,6}$, whose spatial support is shown in C, and whose residuals are shown in D fitted by the frequency peak shown in the periodogram.

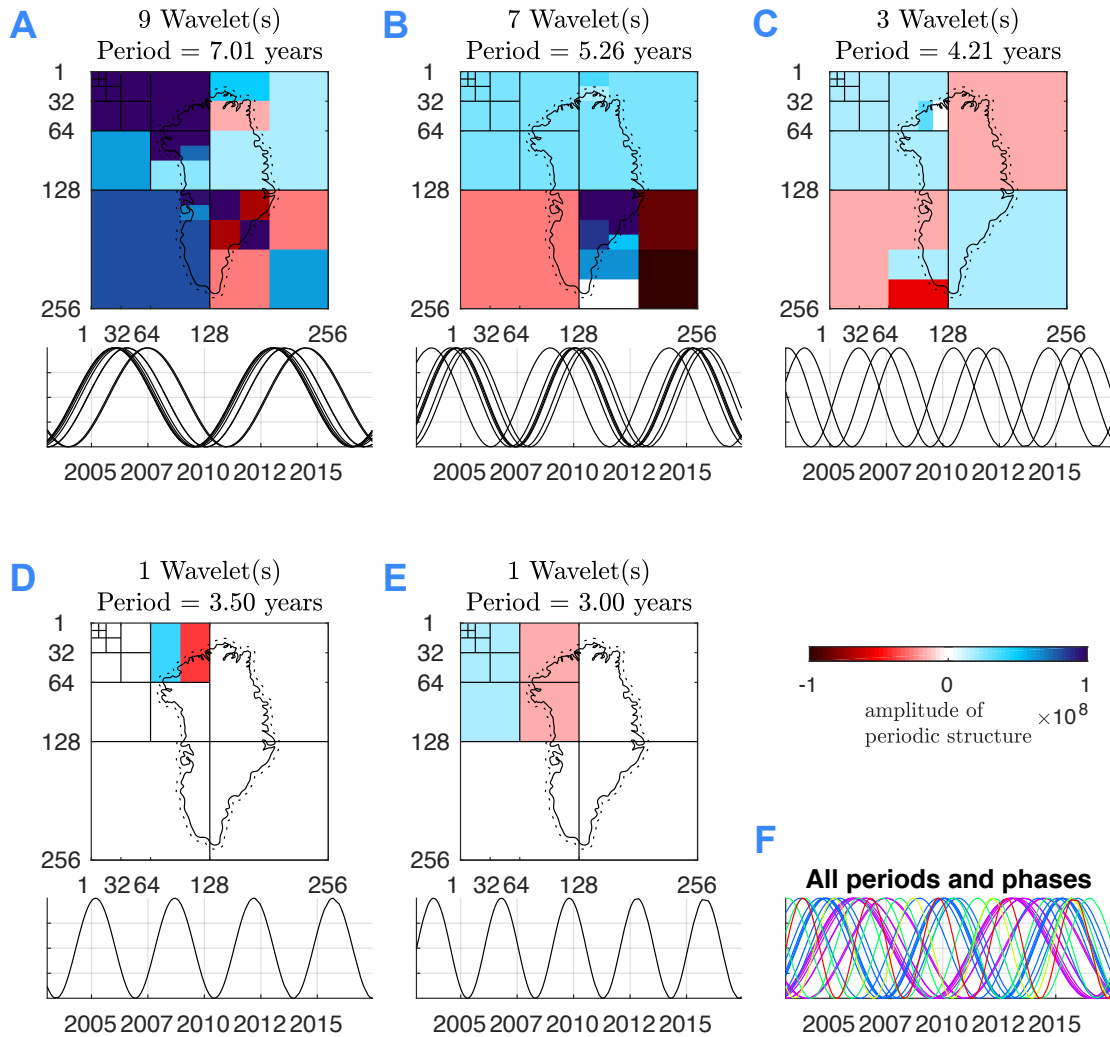


Figure 12: Maps of the wavelets with unexpected periodic structure within the residuals of their modeled coefficients. For each approximate period in the coefficient time series (estimated by Fourier transform), the corresponding wavelets are colored by the amplitude of the spectral power at that frequency in A–E (darker color corresponds to stronger periodic amplitude). Note that there is spatial clustering, in the northwestern and southwestern quadrants of Greenland (A, B, D, & E). Below each period map is a simple graph showing the alignment of phases for the temporal structure of the corresponding coefficients. Note that for the longest two time series, of about 5.25 and 7 years, the phases are generally clustered together, suggesting that the periodic structures result from a coherent mechanism. F shows the superposition of all phases, again with blue and purple representing the strongly clustered longer periods.

Conclusions and Future Work

Wavelet analysis has shown to be a valuable tool in tackling localized gravimetry analysis from spherical harmonic data. Applied to the Greenland Ice Sheet, we have shown that wavelet de-

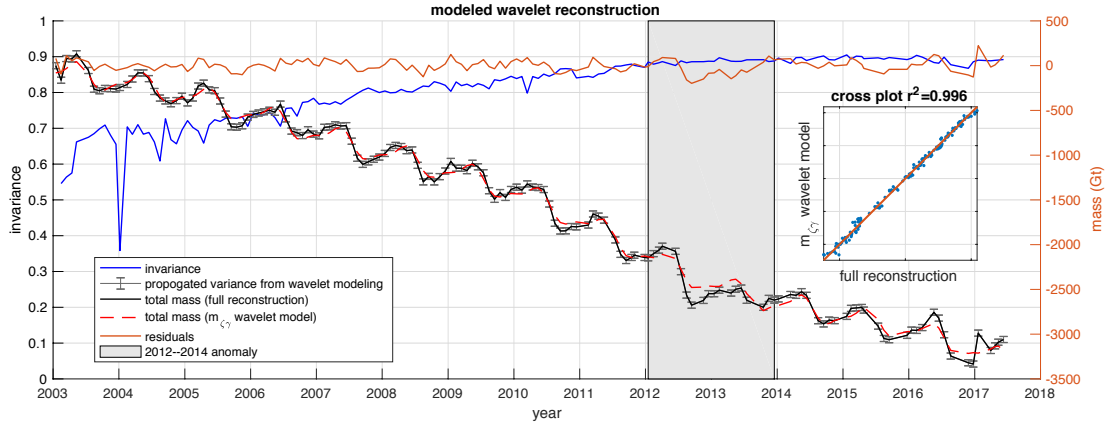


Figure 13: Identical to Figure 10, but with the altered modeled wavelet reconstruction which includes additional periodic oscillations of 7 and 5.25 years (see Figure 12, in dashed red). The invariance measures recovery of spatial structure (blue), approximately (35–70%) in month to month reconstruction (at the beginning of the reconstruction), and very good (approaching 90%) in the beginning to end reconstruction (see Table 3). The residuals are the difference between the full and modeled reconstructions, equal to the $\sum n$ in Equation 2. The error-bars represent 2 standards of deviation with respect to propagated variance from the coefficient model residuals (see Figure 9) and are an estimate of noise and error inherent to the reconstruction (see Figures 1 & 4 for a parallel example in the Spherical harmonic basis). Inset is a cross-plot showing the correlation of the full and modeled reconstructions, improved by 0.4% from the unaltered wavelet reconstruction (see Figure 10). Highlighted in gray are the seasons of 2012–2014 which represent the most significant deviation from the expected behavior of the Greenland Ice Sheet within the GRACE record.

composition in a single basis of 68 wavelets can capture the underlying spatial structure of the melting ice sheet through time with very predictable rates of bias. Modeling of wavelet coefficients can be accomplished through similar inversion techniques as those used in the Slepian basis, however greater information is revealed due to the compact scaling properties of wavelet functions. Specifically, we have found 3–7 year oscillations in mass in several regions of Greenland, which are as of yet unclear in origin. Additionally, we found that we could successfully locate inter-annual variability such as the 2012–2014 deviation to a few specific wavelets, revealing the scale and location of these anomalies.

Moving forward, the locations of oscillations and anomalies revealed in the wavelet basis are expected to be related to local sea-surface temperature, atmospheric pressure, or other climate variables. Understanding the cause of the intriguing results shown here is the crucial step that can both validate our findings and increase our understanding of the Greenland Ice Sheet.

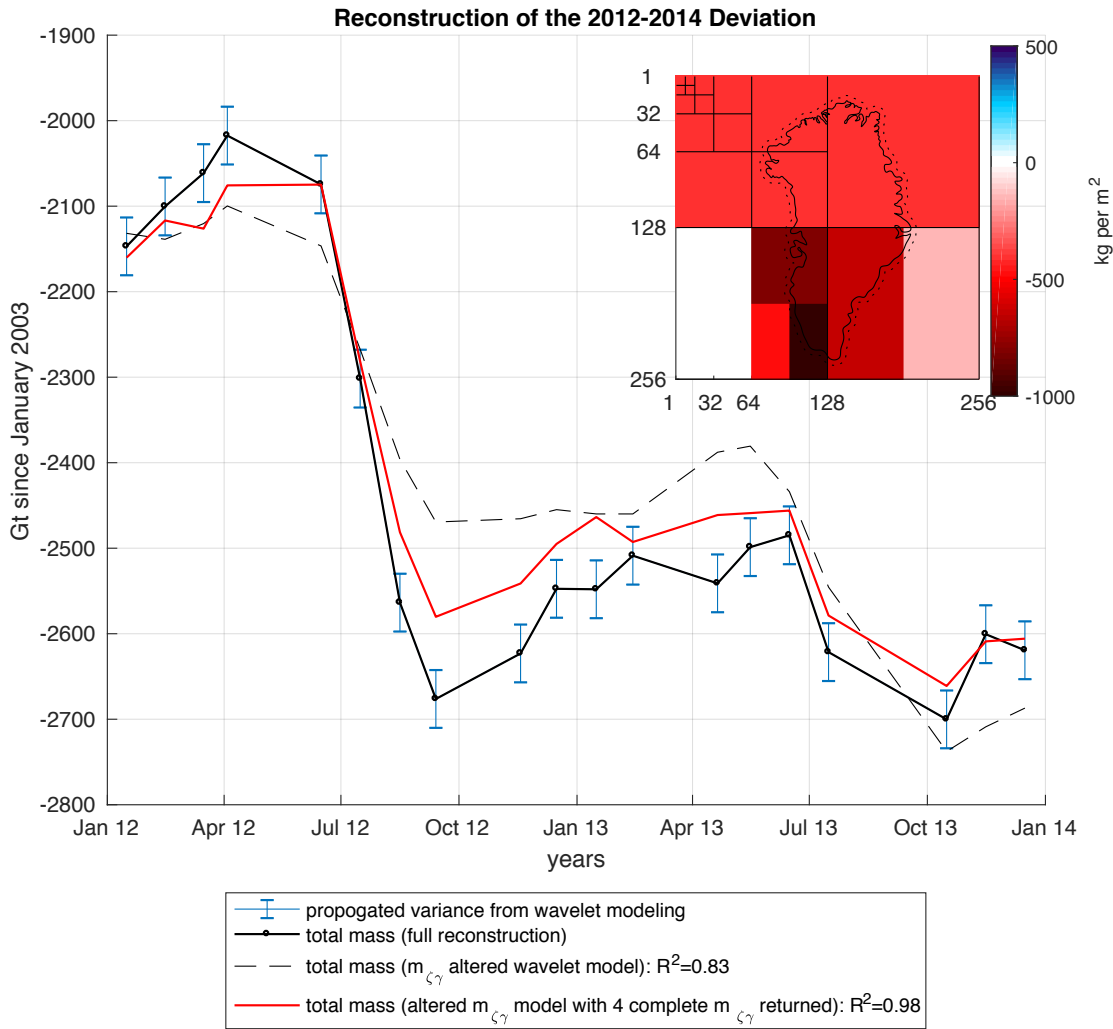


Figure 14: The 2012–2014 deviation in Greenland mass and the total from the reconstructed modeled wavelet coefficients. By adding in the real values of only four wavelet coefficients back into the modeled wavelet reconstruction we improve the variance explanation by 15%. These wavelets are shown inset, weighted by their values in September 2012, the extreme of the deviation, and are concentrated in southwestern Greenland.

Appendix A: Data sources

RL05 spherical harmonic coefficients for the time-variant geopotential field from the GFZ, JPL, and CSR data processing centers are available at:

<ftp://podaac.jpl.nasa.gov/allData/grace/L2/>

Coefficients describing Earth's center of mass (spherical harmonic degree 1, from Swenson et al., 2008) are available at:

ftp://podaac-ftp.jpl.nasa.gov/GeodeticsGravity/tellus/L2/degree_1/

Coefficients describing Earth's oblateness (spherical harmonic degree 2, order 0, from Cheng et al., 2013) are available at:

ftp://ftp.csr.utexas.edu/pub/slrf/degree_2/

MATLAB code for the expansion and manipulation of spherical harmonic eigenfunctions into Slepian bases and manipulation of GRACE files is borrowed and adapted from:

<https://github.com/csdms-contrib/>

Monthly values for the North Atlantic Oscillation Index are calculated by the Climate Prediction Center, with normalized monthly average values since January 1950 available at:

http://www.cpc.ncep.noaa.gov/products/precip/CWlink/pna/nao_index.html

Appendix B: GRACE, spherical harmonics, and Slepian functions

Adapted directly from RESOLVING AND CONTEXTUALIZING THE SIGNAL OF GREENLAND ICE LOSS 2014–2017, by Benjamin Getraer.

The Gravity Recovery and Climate Experiment is a twin-satellite mission active 2002–2017, with its final data collection completed in October 2017. GRACE measurements are made accessible in the form of several data products offered through NASA and partnered agencies, which generally rely on a method of data reduction to translate the “Level 1” GRACE measurements of satellite positions into globally projected mass anomaly estimations. There are two primary methods of data reduction: The creation of “mascons,” roughly equal-area sections around the globe on the scale of single arc-degrees, each assigned a single number representing mass change, and the calculation of spherical harmonic coefficients, which correspond to continuous functions in three dimensions that when summed can model the spatially continuous variation of mass on the surface of Earth. The difference between continuous and discrete data reduction (harmonics vs. mascons) often has to do with localization of the signal in time and space. Discrete solutions may not be able to “see” continuous large scale patterns, while continuous solutions necessarily “hide” information about very localized signals in a collection of globally continuous patterns (see Expansion of the GRACE signal in space and time).

The spherical harmonic method requires continuous functions on Earth’s surface, whereby a field of interest can be developed into a series solution of eigenfunctions $Y_{lm}(\theta, \phi)$, where l refers to the “order” (integers 0 to ∞) and m the “degree” (integers $-l$ to $+l$) of each harmonic (θ and ϕ reference location on the surface of Earth). Due to limitations in computational power and in the spatial resolution of the data being modeled by the harmonic functions, calculated solutions are bandlimited, meaning that they are calculated up to a finite order L . See Simons et al. (2006), their section 3 for a concise summary. See our Figure 15 for illustrations of low-order spherical harmonic eigenfunctions.

Monthly coefficients for bandlimited global spherical harmonic solutions of the time-variable geopotential field are independently calculated by three different processing centers (GFZ in

Comparison of Spherical Harmonic Eigenfunctions to Slepian Basis Eigentapers

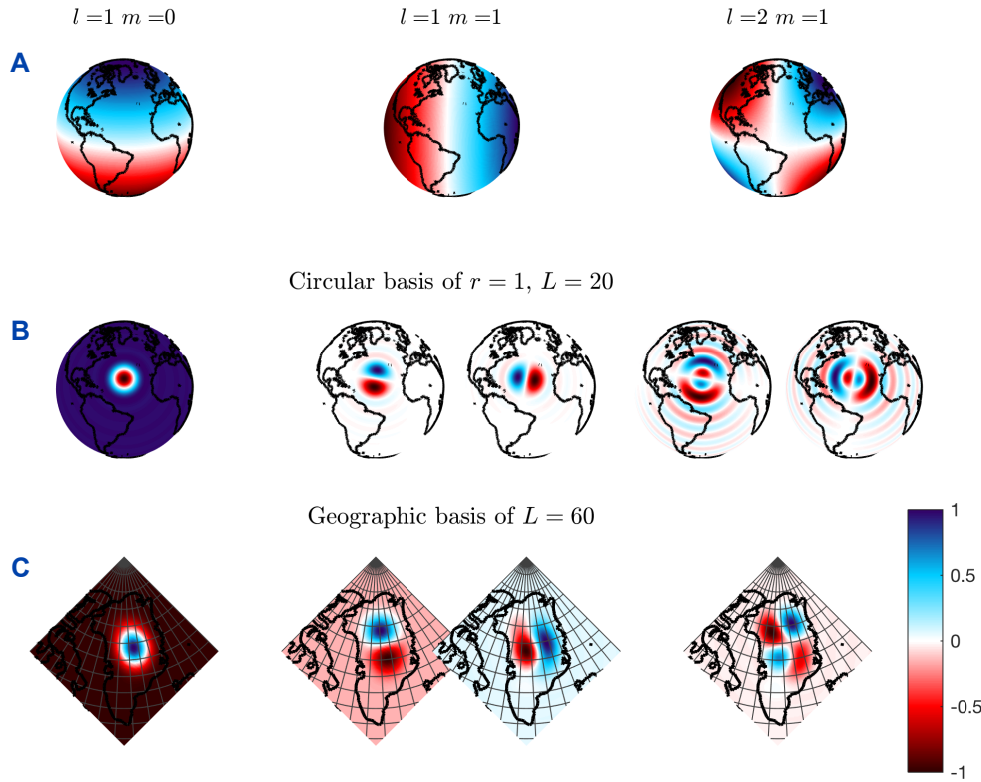


Figure 15: Three low-order spherical harmonic eigenfunctions $Y_{lm}(\theta, \phi)$ are illustrated in **A** as examples of the basic forms these functions take: zonal (left, $m = 0$), sectoral (middle, $m = l$), and tesseral (right, $m \neq l \neq 0$). When expanded into a geographically-localized Slepian basis, the forms of these eigenfunctions have parallel eigentapers as illustrated in rows **B** and **C**. The eigentapers allow for reconstruction of a signal with power concentrated within a geographical basis, minimizing the effect of the signal outside of the basis on the series solution. r is radius, L is the bandlimit of maximum order l used in the Slepian expansion.

Potsdam, Germany; CSR at University of Texas, Austin; JPL at California Institute of Technology) and published publicly as the GRACE Level 2 Release 05 products for a few different bandwidths (see Appendix A: Data sources). The RL05 product is pre-corrected to remove the time-invariant geopotential field using the GRACE Gravity Model 03 (Tapley et al., 2007), and we use coefficients describing Earth's center of mass (spherical harmonic degree 1, from Swenson et al., 2008) and oblateness (spherical harmonic degree 2, order 0, from Cheng et al., 2013) calculated from Satellite Laser Ranging in order to accurately capture mass variations on scales much larger than the area covered by the GRACE satellites (see Appendix A: Data sources). The coefficients are released as contributions to gravitational potential in units of $\frac{\text{kg}^2}{\text{s}^2}$,

and are converted to equivalent surface density on Earth in units of $\frac{\text{kg}}{\text{m}^2}$ using the method of Wahr et al. (1998). Mass estimates are calculated through area-integration, and converted to sea-level equivalence using the method of Tian et al. (2015).

A third method of data reduction uses the spherical harmonic coefficients in a linear combination of their respective functions to constrain explanatory power to an arbitrary geographic location (Simons et al., 2006). This method generates linear combinations of the spherical harmonic eigenfunctions $Y_{lm}(\theta, \phi)$ called scalar Slepian functions $g_\alpha(\theta, \phi)$, where α refers to the “rank” of the Slepian function, which is a single linear combination of all spherical harmonic eigenfunctions up to order L , also referred to as an “eigentaper.” Formally, this expansion is expressed in terms of the spherical harmonic eigenfunctions by:

$$\sum_{l=0}^L \sum_{m=-l}^l f_{lm} Y_{lm}(\theta, \phi) = \sum_{\alpha=1}^{(L+1)^2} f_\alpha g_\alpha(\theta, \phi) \quad (3)$$

By construction the functions $g_\alpha(\theta, \phi)$ are centered around the geographic region of interest. A few eigentapers are concentrated in power strictly within the region, and most are concentrated in power predominantly outside of the region. The signal within the region is approximated by choosing those functions $g_\alpha(\theta, \phi)$ whose ratio of power inside of that region to outside of the region is significant (often around $\geq \frac{1}{2}$), the number of which is referred to as the Shannon number N . The resulting spatially concentrated estimation of the global field is expressed in the approximation:

$$\sum_{l=0}^L \sum_{m=-l}^l f_{lm} Y_{lm}(\theta, \phi) \approx \sum_{\alpha=1}^N f_\alpha g_\alpha(\theta, \phi) \quad (4)$$

Though limited by N , the Slepian expansion is useful by reducing the unnecessary information in the global spherical harmonic coefficients — namely, the signal everywhere else in the world. The method of calculating geographically constrained scalar Slepian functions from a bandlimited series of spherical harmonics, as well as the relationship between the geographical area and the Shannon number is described in mathematical detail by Simons et al. (2006). See our

Figure 15 for illustrations of low-rank Slepian eigentapers in an circular, axisymmetric basis and a Greenland basis.

Slepian-based harmonics have the advantage of continuous solutions as opposed to the coarse rasterized solutions of mascons, with less of the noise and bias associated with globally continuous spherical harmonics. The expansion of global spherical harmonics into a localized Slepian basis of eigentapers allows for locally constrained signals to be extracted from the continuous global GRACE RL05 data product with less impact from noise or signals from other geographic locations, a problem that reduces the precision of the standard spherical harmonic method. We will find localized mass anomaly solutions using the Slepian expansion method of data reduction from the GRACE CSR RL05 $L = 60$ spherical harmonic coefficients (see Harig & Simons, 2012).

Our project builds upon the methods, results, and unresolved questions from previous work done by Chris Harig in the Simons Research Group in the Princeton Department of Geosciences. That work first applied the spherical Slepian basis to the analysis of Greenland ice mass, with results of lower error in both mass estimation and spatial distribution of the geopotential signal than previous studies using different analysis techniques (Harig & Simons, 2012).

References

- Bevis, M., Harig, C., Khan, S. A., Brown, A., Simons, F. J., Willis, M., Fettweis, X., van den Broeke, M. R., Madsen, F. B., Kendrick, E., Caccamise II, D. J., van Dam, T., Knudsen, P., & Nylen, T., 2018. Accelerating changes in ice mass within Greenland, and the ice sheet's sensitivity to atmospheric forcing, *in submission to Proc. Natl. Acad. Sc.*.
- Cadio, C., Panet, I., Davaille, A., Diament, M., MÃ©tivier, L., & de Viron, O., 2011. Pacific geoid anomalies revisited in light of thermochemical oscillating domes in the lower mantle, *Earth and Planetary Science Letters*, **306**(1), 123–135.
- Cheng, M., Tapley, B. D., & Ries, J. C., 2013. Deceleration in the Earth's oblateness, *Journal of Geophysical Research: Solid Earth*, **118**(2), 740–747, doi: 10.1002/jgrb.50058.
- Church, J., Clark, P., Cazenave, A., Gregory, J., Jevrejeva, S., Levermann, A., Merrifield, M., Milne, G., Nerem, R., Nunn, P., Payne, A., Pfeffer, W., Stammer, D., & Unnikrishnan, A., 2013. *Climate Change 2013: The Physical Science Basis. Contribution of Working Group I Contribution to the Fifth Assessment Report of the Intergovernmental Panel on Climate Change*, chap. Sea Level Change, p. doi: 10.1017/CBO9781107415324, Cambridge Univ. Press.
- Enderlin, E. M., Howat, I. M., Jeong, S., Noh, M.-J., van Angelen, J. H., & van den Broeke, M. R., 2014. An improved mass budget for the Greenland ice sheet, *Geophysical Research Letters*, **41**(3), 866–872 doi 10.1002/2013GL059010.
- Harig, C. & Simons, F. J., 2012. Mapping Greenland's mass loss in space and time, *Proc. Natl. Acad. Sc.*, **109**(49), 19934–19937, doi: 10.1073/pnas.1206785109.
- Harig, C. & Simons, F. J., 2015. Accelerated West Antarctic ice mass loss continues to outpace East Antarctic gains, *Earth Planet. Sci. Lett.*, **415**, 134–141, doi: 10.1016/j.epsl.2015.01.029.
- Harig, C. & Simons, F. J., 2016. Ice mass loss in Greenland, the Gulf of Alaska, and the Canadian Archipelago: Seasonal cycles and decadal trends, *Geophysical Research Letters*, **43**(7), 3150–3159,

- doi: 10.1002/2016GL067759.
- Harig, C., Simons, F., Wang, L., & Shum, C., 2012. Localized Inversion of GRACE Level 1B Data Over Greenland Using Slepian Functions, in *AGU Fall Meeting Abstracts*.
- Hartmann, D., Tank, A. K., Rusticucci, M., Alexander, L., Brönnimann, S., Charabi, Y., Dentener, F., Dlugokencky, E., Easterling, D., Kaplan, A., Soden, B., Thorne, P., Wild, M., & Zhai, P., 2013. *Climate Change 2013: The Physical Science Basis. Contribution of Working Group I Contribution to the Fifth Assessment Report of the Intergovernmental Panel on Climate Change*, chap. Observations: Atmosphere and Surface, p. doi: 10.1017/CBO9781107415324, Cambridge Univ. Press.
- Khan, S. A., Aschwanden, A., Bjørk, A. A., Wahr, J., Kjeldsen, K. K., & Kjær, K. H., 2015. Greenland ice sheet mass balance: a review, *Reports on Progress in Physics*, **78**(4), 046801.
- McMillan, M., Leeson, A., Shepherd, A., Briggs, K., Armitage, T. W., Hogg, A., Munneke, P. K., van den Broeke, M., Noël, B., van de Berg, W. J., Ligtenberg, S., Horwath, M., Groh, A., Muir, A., & Gilbert, L., 2016. A high-resolution record of Greenland mass balance, *Geophysical Research Letters*, **43**(13), 7002–7010, doi: 10.1002/2016GL069666.
- Panet, I., Chambodut, A., Diament, M., Holschneider, M., & Jamet, O., 2006. New insights on intraplate volcanism in French Polynesia from wavelet analysis of GRACE, CHAMP, and sea surface data, *Journal of Geophysical Research: Solid Earth (1978–2012)*, **111**(B9).
- Panet, I., Bonvalot, S., Narteau, C., Remy, D., & Lemoine, J.-M., 2018. Migrating pattern of deformation prior to the Tohoku-Oki earthquake revealed by GRACE data, *Nature Geoscience*, p. 1.
- Simons, F. J., Dahlen, F. A., & Wieczorek, M. A., 2006. Spatiospectral concentration on a sphere, *SIAM Rev.*, **48**(3), 504–536, doi: 10.1137/S0036144504445765.
- Swenson, S., Chambers, D., & Wahr, J., 2008. Estimating geocenter variations from a combination of GRACE and ocean model output, *Journal of Geophysical Research: Solid Earth*, **113**(B8), doi: 10.1029/2007JB005338.
- Tapley, B. D., Ries, J. C., Bettadpur, S., Chambers, D., Cheng, M., Condi, F., & Poole, S., 2007. The GGM03 Mean Earth Gravity Model from GRACE, in 88(52), *Fall Meet. Suppl.*, Abstract G42A-03, Eos Trans. AGU.
- Tian, Y., Scaioni, M., Tong, X., & Li, R., 2015. On the Conversion of Antarctic Ice-Mass Change to Sea Level Equivalent, *Marine Geodesy*, **38**(1), 89–97, doi: 10.1080/01490419.2014.969458.
- Vaughan, D., Comiso, J., Allison, I., Carrasco, J., Kaser, G., Kwok, R., Mote, P., Murray, T., Paul, F., Ren, J., Rignot, E., Solomina, O., Steffen, K., & Zhang, T., 2013. *Climate Change 2013: The Physical*

- Science Basis. Contribution of Working Group I Contribution to the Fifth Assessment Report*, chap. Observations: Cryosphere, p. doi: 10.1017/CBO9781107415324, Cambridge Univ. Press.
- Velicogna, I., 2009. Increasing rates of ice mass loss from the Greenland and Antarctic ice sheets revealed by GRACE, *Geophysical Research Letters*, **36**(19), doi 10.1029/2009GL040222, L19503.
- Velicogna, I. & Wahr, J., 2005. Greenland mass balance from GRACE, *Geophysical Research Letters*, **32**(18).
- Wahr, J., Molenaar, M., & Bryan, F., 1998. Time variability of the Earth's gravity field: Hydrological and oceanic effects and their possible detection using GRACE, *Journal of Geophysical Research: Solid Earth*, **103**(B12), 30205–30229.
- Wouters, B., Chambers, D., & Schrama, E. J. O., 2008. GRACE observes small-scale mass loss in Greenland, *Geophysical Research Letters*, **35**(20).
- Zwally, H. J., Giovinetto, M. B., Beckley, M. A., & Saba, J. L., 2012. Antarctic and Greenland Drainage Systems, *GSFC Cryospheric Sciences Laboratory*.